Latin American Journal of Solids and Structures
www.lajss.org

Dynamic analysis and vibration control of a multi-body system using MSC Adams

Abstract

In this paper, modelling and simulation of a multi-body system for its vibration control using sensors and actuators is presented. The model developed on MSC ADAMS consists of six legs connecting moving and base plates using spherical joints with axial rotation of legs constrained. It contains linear actuator collocated with force sensor. Mathematical model of the mechanism representing the Kinematic and Dynamic analysis of model is presented. The Leg Length variation obtained using MATLAB is obtained in order to validate the model developed in MSC ADAMS. Natural frequencies for six different mode shapes are obtained from vibration excitation analysis. A decentralized force feedback controller which uses PID control law with single gain is used for actively attenuating the vibration, which is coming from base platform. The transfer function, defined as the ratio of Laplace transformation of the acceleration of moving plate and base plate, is considered as a measure of isolation. Effect of proportional, derivative and integral feedback is studied separately and together as well. A significant isolation in the resonance transmissibility and natural frequency of the mechanism is demonstrated.

Keywords

Platform; vibration control; force sensor; linear actuator; PID controller.

M. Naushad Alam[a]
Adnan Akhlaq[b]
Najeeb ur Rahman[c]

[a,b,c]Department of Mechanical Engineering, Aligarh Muslim University, Aligarh,U.P-202002, India.

Corresponding author:
[a]naushad7863@rediffmail.com
[b]adnanakhlaq@gmail.com
[c]najeebalig@rediffmail.com

http://dx.doi.org/10.1590/1679-78251598

Received 23.09.2014
Accepted 20.04.2015
Available online 02.05.2015

1 INTRODUCTION

Vibrations propagating into the mechanical systems can cause many problems at different levels causing performance degradation for sensitive systems. Vibrations accompany us everywhere and in most cases these vibrations are undesirable. The adverse effect of these vibrations can range from negligible to catastrophic depending on the severity of the disturbance and the sensitivity of the equipment (Abu Hanieh et al., 2002). Vibration control techniques have been developed to provide dynamic protection to all types of equipment from undesirable effect of vibrations.

The Stewart parallel mechanism (Stewart, 1965) has the capability to control the six degrees of freedom of a rigid body, and has proven to be of high positioning accuracy. So, the Stewart parallel mechanism is chosen to stabilize the receivers of the telescope. The Stewart parallel mechanism in this application has two platforms, one is the platform to be stabilized, and the other is the base platform that is mounted on the cable-car. When the base platform vibrates with wind-induced cable-car, the vibrations of the stabilized platform can be alleviated by adjusting the six actuators with appropriate control laws. Most of the available studies on dynamics and control of Stewart platform (Geng et al., 1992; Lebret et al., 1993; Dasgupta and Mruthyunjaya, 1998; Liu et al., 2000; Gallardo et al., 2003; Mukherjee et al., 2007; Lopes, 2009; Li et al., 2012) deals with the case that the base platforms are fixed but for this application the dynamics and control of the mechanism are different from the available analyses.

Stewart Platform Mechanisms have been investigated for many years as six DOF motion generators and six DOF parallel link manipulators. The Stewart Platform is one of the most popular parallel manipulators requiring least number of actuators to generate six degree-of freedom, high load carrying capacity, robust kinematics and dynamic behavior with absence of error-summation issues as is in serial manipulator makes it suitable choice for a number of applications including aerospace and defense, automotive, transportation, machine tool technology, and recently medical applications. Broadly its applications are for precise pointing and motion manipulation. Motion manipulation category includes the vibration isolation wherein the disturbance propagating from base to moving or vice versa through the legs is attenuated by the integrated sensor and actuators.

Hongling et al. (2007) discusses typical problems in active vibration isolation systems and compares the control force, feedback gain, and actuator stroke of several passive-active vibration isolation systems. In order to improve the performance of the active isolation systems a joint vibration reduction method that combines an active vibration isolation system and an adaptive dynamic vibration absorber are also discussed in the paper. Geng and Haynes (1993), Graf and Dillmann (1997) and Cobb et al. (1999) have investigated the use of Stewart Gough platform for vibration isolation, but they are concentrated on vibrations of small amplitude and as the inertia of the base is much higher than that of the payload, the couple effect of the two platforms is not prominent.

Preumont et al. (2007) presented a six-axis vibration isolator for space applications by considering the decentralized feedback control approach which has attractive robustness properties. Kapur et al. (2007) brought out a method wherein the instantaneous gain in the degrees of freedom of mechanisms at singular configurations can be completely overcome by an appropriate choice of flexural joints in the place of regular joints. Liu and Benli (2008) presented the use of hybrid isolators for active vibration control of the flexure struts of Stewart platform. Dynamic performance of the system depends both on the control parameters as well as the physical parameters of the system. Wang et al. (2009) proposed an optimal design method to expand the bandwidth for the control of large hydraulic Stewart platform. The method is based on generalized natural frequency and takes hydraulic oil into consideration. They presented Lagrangian formulation which considers the whole leg inertia to obtain the accurate equivalent mass matrix.

Hoque et al. (2010) presented a six-degree-of-freedom hybrid vibration isolation system integrated with an active negative suspension, an active–passive positive suspension and a passive weight support mechanism in order to develop a six-axis vibration isolation system using active zero-power controlled magnetic suspension. Hajimirzaalian et al. (2010) have shown the comparison between the inverse

dynamic solution based on Lagrangian formulation and the direct dynamic solution of the Stewart platform by simulation with ADAMS. Fehr and Eberhard (2011) considered nonmodal model reduction techniques for flexible multibody systems within the floating frame of reference framework. In their work, they have presented four different possibilities of modeling appropriate interface points to reduce the number of inputs and outputs.

Hoque et al. (2011) proposes a module-type three-degree-of-freedom vibration isolation system for a parallel mechanism using modified zero-power control. Li et al. (2012) proposed a hybrid manipulator applied to vibration isolation of the manufacturing systems in which the translations and rotations of the manipulator are decoupled, so the proposed isolator can isolate vibrations with wide range of frequency. Hayat et al. (2012) presented the design and analysis of a compliant mechanism using hyperbolic flexural hinges. Hajimirzaalian et al. (2013) presented the dynamic analysis and simulation for a nonlinear model of a Stewart platform with asymmetric-adjustable payload, based on Lagrangian approach. The system has been modelled in ADAMS engineering software and the inverse dynamic solution has been developed by both analytical (Lagrangian formulation) and simulation (ADAMS) methods. Furqan and Alam (2013) designed and analysed a complete positioning system of Stewart Platform that consists of top plate (moving platform), a bottom plate (fixed base), and six extensible legs connecting the top plate to the bottom plate. In order to achieve better accuracy over commonly used universal and spherical joints the flexible joints have been employed. Xia et al. (2014) established a driveline dynamic model of the RWD vehicle by multi-body dynamic method. They calculated the natural frequencies and modal shapes for each gear position and predicted torsional vibration responses by forced vibration analysis. Zhang et al. (2014) presented the first-order approximation coupling model of planar 3-RRR flexible parallel robots, in which the rigid body motion constraints, elastic deformation motion constraints, and dynamic constraints of the moving platform are considered.

In this paper modeling and Simulation of Stewart Platform for vibration control using sensor and actuator is presented. The inverse and forward kinematic analysis is done and code is developed in order to validate the results of the model developed in MSC ADAMS. The moving and fixed platforms provided in Harib and Srinivasan (2003) is considered to compare the results. The model has been developed on MSC ADAMS using geometric and inertia properties of the different parts of the model. Analysis for vibration exciter was done by providing a sinusoidal base excitation of 25 milli g in all three orthogonal axes. A decentralized force feedback controller using PID control law with single gain has been used for actively attenuation the vibration coming from base platform. Finally the simulation results for vibration excitation and vibration isolation is presented. Effect of proportional, derivative and integral feedback is also studied separately and together as well

2 DESCRIPTION OF THE MODEL

Figure 1 shows a spatial 6-dof, 6 SPS parallel manipulator having six identical limbs connecting the moving platform to the fixed base through spherical joints at points B_i and A_i, for $i = 1, 2...6$ respectively. To fully describe its position and orientation, six coordinates are needed. The X-Y-Z coordinate frame is fixed to the stationary base at point O_A, the centre of the base plate. The u-v-w coordinate frame is attached to the payload platform at the centre point O_B and moves with the payload platform.

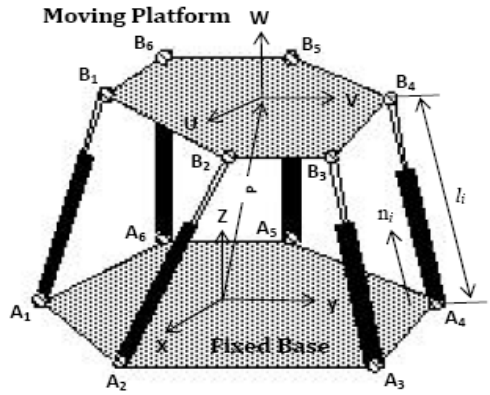

Figure 1: Schematic diagram of Stewart Platform.

In the nominal position, the X-Y-Z fixed base coordinate system is co-aligned with the moveable u-v-w coordinate frame but is offset by the vector p, whose magnitude is the separation distance between the payload platform and the base plate, and whose direction is along the +Z-axis. The vector aligned with each actuator, l_i had a magnitude equal to the length of that actuator. The vector a_i is from the fixed origin $\mathrm{O_A}$ to the corresponding A_i joint. The vector ${}^{\mathrm{B}}\mathrm{b}_i$ is from the moving platform origin $\mathrm{O_B}$ to the $\mathrm{B}i$ joint in the payload frame, u-v-w ($\mathrm{b}i$ in fixed X-Y-Z frame).

The moving platform is a rigid body that possesses six degrees of freedom. To fully describe its position and orientation, six coordinates are needed. Three of these coordinates are positional displacements that locate the position of a reference point in the moving platform with reference to a fixed coordinate system. The other three coordinates are angular displacements that describe the orientation of the moving platform with reference to a nonrotating coordinate system. Euler angles are used to represent rigid body kinematics and dynamics. The set of Euler angles (ϕ, θ, ψ) which uniquely determine the orientations of a rigid body are used. The frame X'Y'Z' as in Harib and Srinivasan (2003) is a nonrotating coordinate system that translates with the rigid body while frame xyz is a body coordinate system that both rotates and translates with the rigid body.

A generalized coordinate vector q, whose elements are the six variables, is chosen to describe the position and orientation of the platform, as

$$q = \left(X,\ Y,\ Z,\ \phi,\ \theta,\ \psi\right)^T \tag{1}$$

The joint space coordinate vector $\boldsymbol{l}$ is defined as

$$\boldsymbol{l} = \left(l_1,\ l_2,\ l_3,\ l_4,\ l_5,\ l_6\right)^T \tag{2}$$

where l_i for $i = 1, \ldots, 6$ are the lengths of the six numbered links of the Stewart Platform.

3 KINEMATIC AND DYNAMIC ANALYSES

In this section Kinematic analysis is performed to determine the manipulator motion as constrained by the geometry of the links. The kinematic analysis is done without considering to the forces or

torques that cause or result from the motion. The dynamic analysis of the multi-body system of the platform is carried out in terms of the Newton–Euler equations.

3.1 Kinematic analysis

A 3x3 rotation matrix ${}^{A}R_{B}$ involving the three Euler angles ϕ, θ, ψ is used for mapping between x-y-z reference frame and X'-Y'-Z' reference frame. ${}^{A}R_{B}$ is given for the used Euler angle representation as

$$ {}^{A}R_{B} = \begin{pmatrix} c\psi c\phi - c\theta s\phi s\psi & -s\psi c\phi - c\theta s\phi c\psi & s\theta s\phi \\ c\psi s\phi + c\theta c\phi s\psi & -s\psi s\phi + c\theta c\phi c\psi & -s\theta c\phi \\ s\psi s\theta & c\psi s\theta & c\theta \end{pmatrix} \tag{3} $$

where c and s denote cosine and sine respectively. The angular velocity and angular acceleration of the moving platform with reference to frame W as functions of the first and second time derivatives of the Euler angles is given by

$$ \omega = \begin{pmatrix} \omega_x \\ \omega_y \\ \omega_z \end{pmatrix} = \begin{pmatrix} 0 & c\phi & s\phi c\theta \\ 0 & s\phi & -c\phi s\theta \\ 1 & 0 & c\theta \end{pmatrix} \begin{pmatrix} \dot{\phi} \\ \dot{\theta} \\ \dot{\psi} \end{pmatrix} \tag{4} $$

and

$$ \alpha = \begin{pmatrix} \alpha_x \\ \alpha_y \\ \alpha_z \end{pmatrix} = \begin{pmatrix} 0 & c\phi & s\phi s\theta \\ 0 & s\phi & -c\phi s\theta \\ 1 & 0 & c\theta \end{pmatrix} \begin{pmatrix} \ddot{\phi} \\ \ddot{\theta} \\ \ddot{\psi} \end{pmatrix} + \begin{pmatrix} 0 & -\dot{\phi}s\phi & \dot{\phi}c\phi s\theta + \dot{\theta}s\phi c\theta \\ 0 & \dot{\phi}c\phi & \dot{\phi}s\phi s\theta - \dot{\theta}c\phi c\theta \\ 0 & 0 & -\dot{\theta}s\theta \end{pmatrix} \begin{pmatrix} \dot{\phi} \\ \dot{\theta} \\ \dot{\psi} \end{pmatrix} \tag{5} $$

Referring to Figure 1, the coordinates of the i^{th} attachment point b_i on the moving platform, given with reference to frame of moving platform as ${}^{B}b_i = \left(u_{b_i}, v_{b_i}, w_{b_i}\right)^{T}$, are obtained with reference to the world coordinate system (i.e. the coordinate system of fixed base) by using

$$ b_i = p + {}^{A}R_{B}\,{}^{B}b_i \tag{6} $$

Once the position of the attachment point b_i is determined, the Leg length vector (L_i) of link is simply obtained by taking the difference of attachment points on moving and base platform with reference to fixed frame. The length of link (l_i) will be simply obtained by taking the magnitude of leg length vector and the unit vector (n_i) along the axis of the prismatic joint of link from base to moving platform is computed by dividing the leg length vector by its magnitude.

3.2 Jacobean analysis

The velocity of point b_i is obtained by differentiating Eq. (6) with respect to time

$$ \dot{b_i} = \dot{p} + \omega \times {}^{A}R_{B}\,{}^{B}b_i \tag{7} $$

The projection of this velocity vector on the axis of the prismatic joint of link i yields the extension rate of link i

$$\dot{l}_i = \dot{b}_i \cdot n_i = \dot{p} \cdot n_i + \omega \times \left({}^{A}R_B \, {}^{B}b_i \right) \cdot n_i \tag{8}$$

or

$$\dot{l}_i = \dot{p} \cdot n_i + \omega \cdot \left({}^{A}R_B \, {}^{B}b_i \right) \times n_i \tag{9}$$

For the purpose of deriving the inverse Jacobian matrix of the Stewart Platform, it is useful to write Eq. (9) for the six links, in matrix form, as

$$\dot{l} = J_1^{-1} \begin{pmatrix} \dot{p} \\ \omega \end{pmatrix} \tag{10}$$

where

$$J_1^{-1} = \begin{pmatrix} n_1^T & \left({}^{A}R_B \, {}^{B}b_1 \times n_1 \right)^T \\ \vdots & \vdots \\ n_6^T & \left({}^{A}R_B \, {}^{B}b_6 \times n_6 \right)^T \end{pmatrix} \tag{11}$$

Using the generalized coordinate the equation is reduced to provide the Jacobian matrix of the machine.

$$\dot{l} = J_1^{-1} J_2^{-1} \dot{q} = J^{-1} \dot{q} \tag{12}$$

where

$$J_2^{-1} = \begin{pmatrix} I_{3\times3} & & O_{3\times3} & \\ & 0 & c\phi & s\phi s\theta \\ O_{3\times3} & 0 & s\phi & -c\phi s\theta \\ & 1 & 0 & c\theta \end{pmatrix} \tag{13}$$

where c and s denote cosine and sine respectively.

3.3 Dynamic analysis

Referring to Figure 2, the accelerations of the centers of mass of part 1 (the moving part) and part 2 (the stationary part) are given by

$$a_{i1} = \left(l_i - l_1 \right) \omega_i \times \left(\omega_i \times n_i \right) + \left(l_i - l_1 \right) \alpha_i \times n_i + 2\omega_i \times \dot{l}_i n_i + \ddot{l}_i n_i \tag{14}$$

$$a_{i2} = l_2 \omega_i \times \left(\omega_i \times n_i \right) + l_2 \alpha_i \times n_i \tag{15}$$

where l_1 and l_2 are the lengths between the centres of mass of parts 1 and 2 and the attachment points a_i and b_i, respectively.

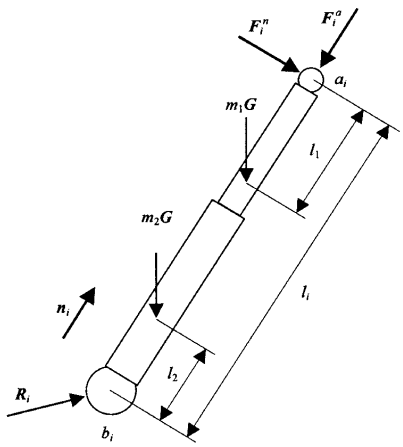

Figure 2: Force components on i^{th} link with two frictionless spherical joints.

Let the reaction force of the platform acting on link i be resolved into two components, as shown in Figure 2, one component F_i^a along the prismatic joint axis of link i, and the other component F_i^n normal to the joint axis. It is assumed that the force component F_i^n and the reaction moment M_i transmitted through the universal joint to find the force component F_i^a

$$F_i = F_i^a + F_i^n \tag{16}$$

where normal component force and axial component force are given by

$$F_i^n = \left(N_i \times n_i - m_i c_i \times n_i\right) \Big/ l_i \tag{17}$$

and

$$F_i^a = f_i^a n_i \tag{18}$$

f_i^a contains the magnitude and sign of F_i^a. The six scalar quantities f_i^a for $i = 1,\ldots,6$ can be determined from the summation of the force and moment components acting on the platform which will result in Newton's equation for the platform as

$$-\sum_{i=1}^{6} f_i^a n_i - \sum_{i=1}^{6} F_i^n + m_p G = m_p \ddot{x}_g \tag{19}$$

Taking the moments about the platform reference point, Euler's equation for the platform gives

$$m_p \overline{r} \times G - \sum_{i=1}^{6} f_i^a \, {}^A R_B \, {}^B b_i \times n_i - \sum_{i=1}^{6} {}^A R_B \, {}^B b_i \times F_i^n - \sum_{i=1}^{6} M_i = \overline{I}_p \alpha - \overline{I}_p \omega \times \omega + m_p \left(\overline{r} \times \ddot{x}_g\right) \tag{20}$$

where m_p is the mass of the platform, $\ddot{x}_g$ is the acceleration of the platform center of mass and $\overline{I}_p$ is the mass moments of inertia of the platform with reference to the world frame W at the center of mass of the platform. $\ddot{x}_g$ is determined in terms of the platform motion variables as

$$\ddot{x}_g = \ddot{x} + \alpha \times \overline{r} + \omega \times \left(\omega \times \overline{r}\right) \tag{21}$$

Eqs. (19) and (20) make a system of 6 linear equations in f_i^a for $i = 1$ to 6. They can be solved for f_i^a as

$$\begin{pmatrix} f_1^a \\ \vdots \\ f_6^a \end{pmatrix} = J_1^T C \tag{22}$$

where we use the matrix ${J_1}^{-1}$ as given by Eq. (11), and define the known vector C as

$$C = \begin{Bmatrix} m_p G - m_p \ddot{x}_g - \sum_{i=1}^{6} F_i^n \\ m_p \overline{r} \times G - m_p \left(\overline{r} \times \ddot{x}_g\right) - \overline{I}_p \alpha + \overline{I}_p \omega \times \omega - \sum_{i=1}^{6} {}^A R_B \, {}^B b_i \times F_i^n - \sum_{i=1}^{6} M_i \end{Bmatrix} \tag{23}$$

Once the interaction forces between the struts and the moving platform are determined, we proceed to compute the actuation forces f_i that power the prismatic joints. This force component will be the axial force that the ball screw exerts on the nut for the electromechanical actuation considered. f_i is determined by summing the axial force components acting on the inner strut tube and nut, which is given by

$$f_i = m_1 a_{i1} \cdot n_i - f_i^a - m_1 G \cdot n_i \tag{24}$$

The joint space force vector F, containing the six actuation force components f_i for $i = 1$ to 6, can be written as

$$F = \left(f_1 \ldots f_6\right)^T \tag{25}$$

Using Eq. (24), F can be obtained as

$$F = \begin{pmatrix} m_1 \left(a_{11} - G\right).n_1 \\ \vdots \\ m_1 \left(a_{61} - G\right).n_6 \end{pmatrix} - J_1^T C$$

On the other hand, the Cartesian space force/torque vector can be obtained using the Jacobian matrix J as

$$\tau = J^{-T} F \text{ or} \tag{26}$$

$$\tau = J^{-T}\begin{pmatrix} m_1\left(a_{11} - G\right).n_1 \\ \vdots \\ m_1\left(a_{61} - G\right).n_6 \end{pmatrix} - J_2^{-T}C \tag{27}$$

where J_2^{-T} is given by Eq. (13)

4 MODELING OF MULTIBODY SYSTEM USING MSC ADAMS

A parametric model is developed in MSC ADAMS environment. The parametric model variables $\begin{bmatrix} R_b & r_m & t & \theta_b & \theta_m \end{bmatrix} = \begin{bmatrix} 0.18 \text{ m} & 0.17 \text{ m} & 0.12 \text{ m} & 0.3 \text{ rad} & 0.5 \text{ rad} \end{bmatrix}$ are used to generate an initial geometric model. Legs contain sensors and actuator and two frictionless spherical joints connecting top and base platforms. Legs are modeled by two rigid bodies connected by a frictionless sliding joint. The actuator and sensors are embedded into lower part of the leg as can be seen in Figure 3. The payload is rigidly connected to moving platform with the geometric centre lying on the lateral axis of the platform. The moving platform is provided with central hole to save the weight. The base platform is modeled as ring wherein all the legs are attached. For simulation studies base platform is modeled as heavy mass much more than the system mass of the order of 10^3 kg.

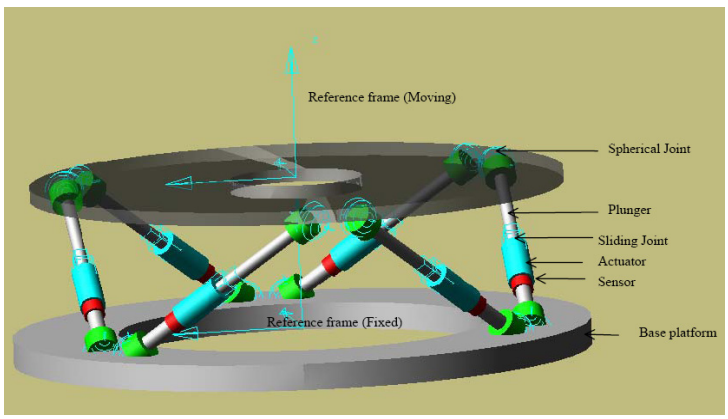

Figure 3: MSC ADAMS Model of S-G Mechanism.

4.1 Validation of the developed simulation model

In order to validate the simulation model a MATLAB code is developed based on the mathematical formulation discussed in section 3. The numerical values for the coordinates of attach points at moving and fixed platforms provided in Harib and Srinivasan (2003) is first used to validate the mathematical formulation.

Parameter	b_1 (m)	b_2 (m)	b_3 (m)	b_4 (m)	b_5 (m)	b_6 (m)
U	0.225	0.1125	-0.1125	-0.225	-0.1125	-0.1125
V	0.0	0.1949	0.1949	0.0	-0.1949	-0.1949
W	-0.228	-0.228	-0.228	-0.228	-0.228	-0.228

Table 1: Attachment points on the moving platform with reference to O_B.

	a_1 (m)	a_2 (m)	a_3 (m)	a_4 (m)	a_5 (m)	a_6 (m)
X	1.7580	1.6021	-1.7580	-1.6021	0.0	0.0
Y	2.8	3.07	2.8	3.07	2.8	3.07
Z	-1.015	-0.925	-1.015	-0.925	2.03	1.85

Table 2: Attachment points on the base platform with reference to O_A.

The position and orientation of the platform are given as:

$$q = \begin{bmatrix} 0.2 & 0.3 & -0.4 & 0.1 & -1.4 & 0.1 \end{bmatrix}^T \tag{28}$$

where the linear displacements are given in meters and the angular displacements are given in radians.

Using the position and orientation of the platform the Kinematic Analysis is performed through the use of MATLAB and the results of leg lengths of six legs obtained are compared well with the results obtained by Harib and Srinivasan (2003) which is shown in Table 3. The comparison of the results presented thus validates the mathematical formulation which will be further used for validating the simulation model developed on MSC ADAMS.

	Leg Length (m)	
Leg	Present Value	Harib and Srinivasan (2003)
1	3.0513	3.0508
2	3.2327	3.2324
3	3.2994	3.2997
4	3.4565	3.4560
5	3.5791	3.5797
6	3.6938	3.6935

Table 3: Leg Lengths of Stewart Gough Mechanism obtained from Kinematic Analysis.

Now, when a time varying position and orientation is given the Kinematic results of leg lengths obtained using MSC ADAMS are compared with the result of MATLAB. A very good comparison of the results is presented in Figure 4. Upon comparison of the result, the simulation model developed in MSC ADAMS is validated and the model will further be used to obtain the simulation results of vibration isolation results.

5 SIMULATION RESULTS

5.1 Analysis for vibration excitation

The normal mode analysis is carried out with a stiffness of 1E5 N/m assigned to legs using spring and with geometric and inertial properties provided to different parts of the model. When the model is provided a base excitation in the form of acceleration at the geometric centre of base platform as sine sweep of constant magnitude of 25 milli g up to 1000 Hz., six different mode shapes are obtained as shown in Figure 5-6. Figure 5 shows one of the two bending mode shapes which are similar about

lateral axis. The natural frequencies of the two bending mode are 15.7224 and 15.796 Hz. Figure 6 shows the plunge mode wherein vibration is about longitudinal axis and the natural frequency is 22.0192 Hz. The shear modes shown in Figure 7 are not purely shear as there is small offset in the CM of the payload and thus it is loosely coupled with bending also. The natural frequencies of the two shear mode are 33.2412 and 33.6565 Hz. Figure 8 represents the torsional mode shape having natural frequency of 38.2003 Hz where it is rotating about Z-axis. This mode is least likely to be excited thus in spite of being near the disturbance frequency does not pose any problem. All the Eigen values are pure imaginary as no passive damping at this point has been introduced in the system.

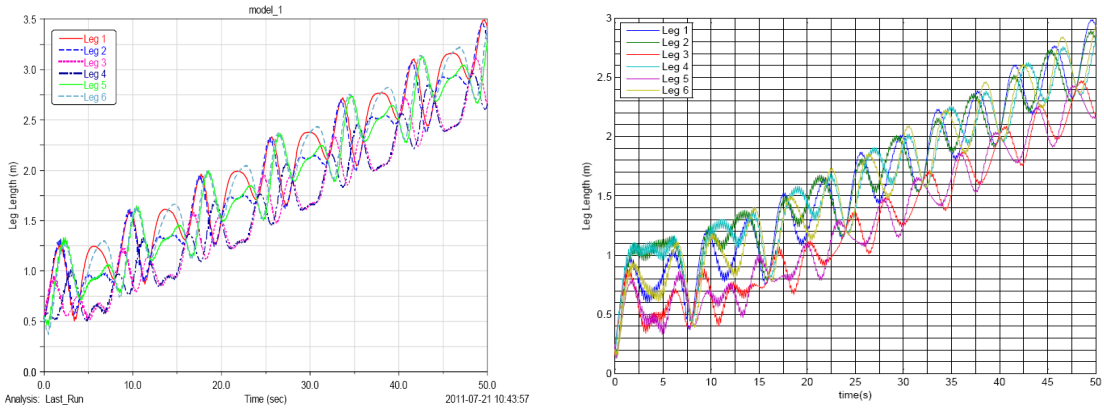

Figure 4: Leg Lengths of six legs (i) using MatLab, (ii) using Adams.

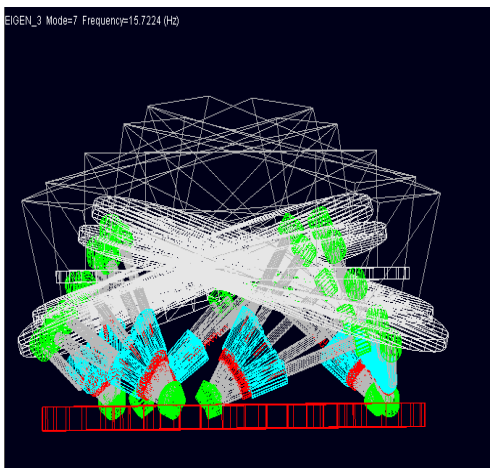

Figure 5: Bending Mode.

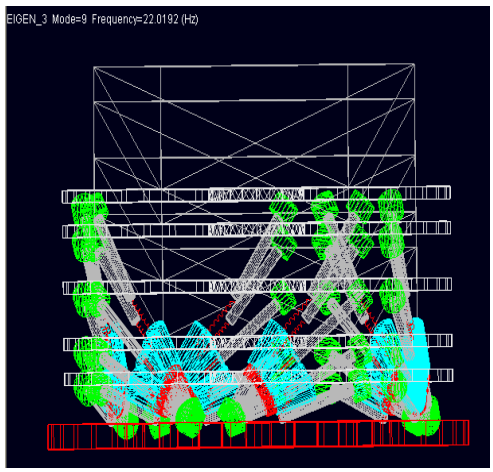

Figure 6: Plunge Mode.

5.2 Response of Stewart Platform to quasi static loads

Inertia load that comes on the Stewart Platform due to input acceleration applied at CG of base plate can be decomposed into two components one fluctuating part called dynamics load and the other called quasi static that is the mean over which dynamic part fluctuates. The response in change in length of legs is recorded when the platform is subjected to ramp acceleration of 20 g is applied in each axis separately.

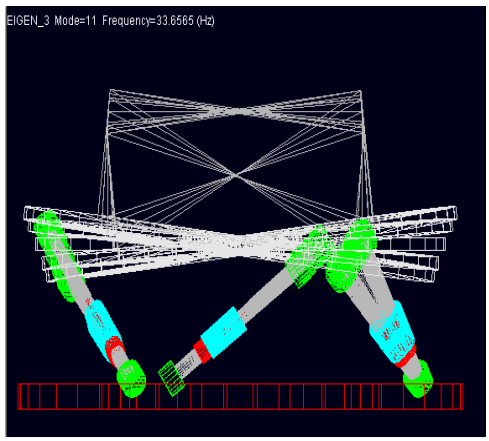

Figure 7: Shear Mode.

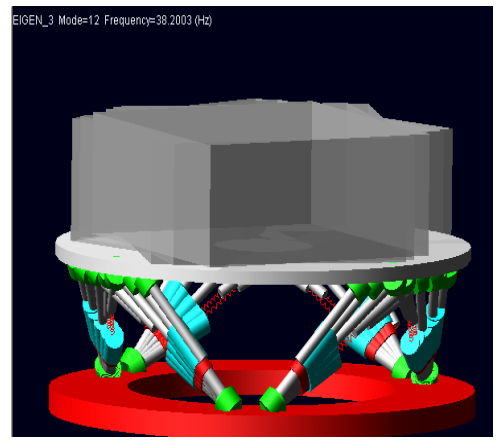

Figure 8: Torsional Mode.

5.2.1 Response of Stewart Platform due to input in X axis

A ramp of acceleration of 20 g is applied at the CG of base platform in X axis direction. The elongations of the legs without control action are presented in Figure 9. The maximum extension and compression is 12 mm and 11 mm, respectively. The legs can be made stiffer using additional springs or soft stopper (made of viscoelastic material rubber etc.) that will become functional only when elongation/compression of the legs extends beyond the specified limits. The resisting forces coming from the springs alone are shown in the Figure 10.

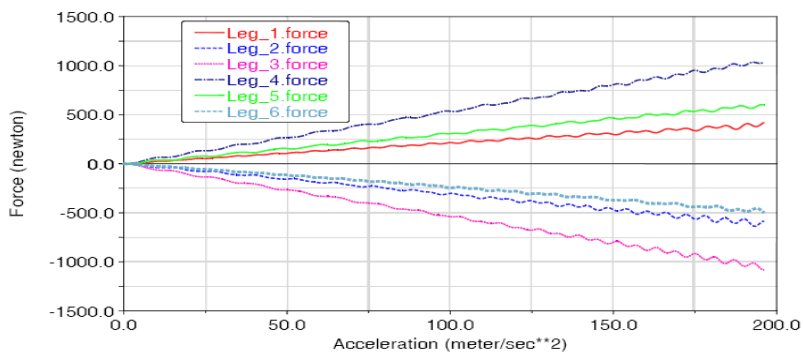

Figure 9: Elongation of Legs due to Input Acceleration in X axis.

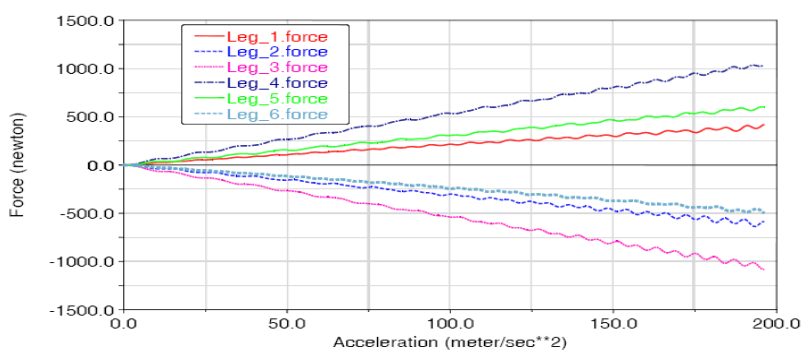

Figure 10: Spring Forces Resisting the QSL Loads in X axis.

The input acceleration given to base and the output acceleration at the centre of moving platform in the same direction is plotted in the Figure 11 which shows nearly rigid behavior with exception of small fluctuations that is because of elastic spring.

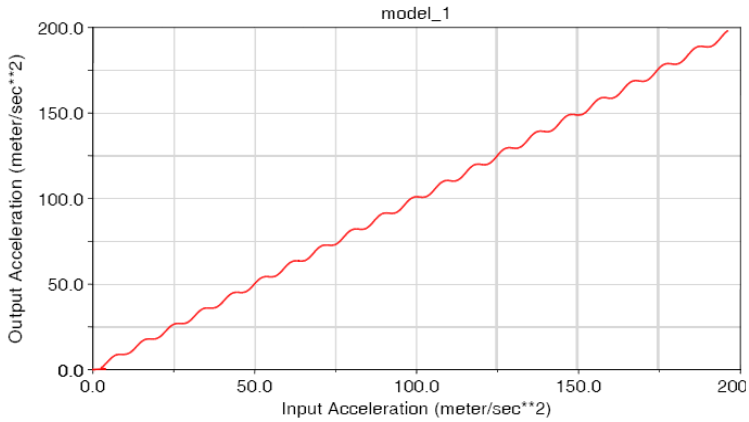

Figure 11: Response of Output Acceleration of Moving Platform in X axis.

5.2.2 Response of Stewart Platform due to input in Z axis

Like X-axis again a ramp acceleration of 20 g is applied at the CG of the base platform in direction of Z-axis. Figures 12-14 show the deformations of legs, forces and output acceleration of moving platform in the excitation direction. The Figure 12 shows that the legs are under compression as is obvious. It undergoes nearly 7 mm compressions in absence of any additional provision meant for restricting the excessive elongation. The resisting forces shown in Figure 13 are responsible for integrity of structures against inertial load is supported by legs-spring of stiffness 1E5 N/m.

The input acceleration given to base and the output acceleration at the center of moving platform in the same direction is plotted in the Figure 14 which shows nearly rigid behavior with exception of small fluctuations that is because of spring action of the legs.

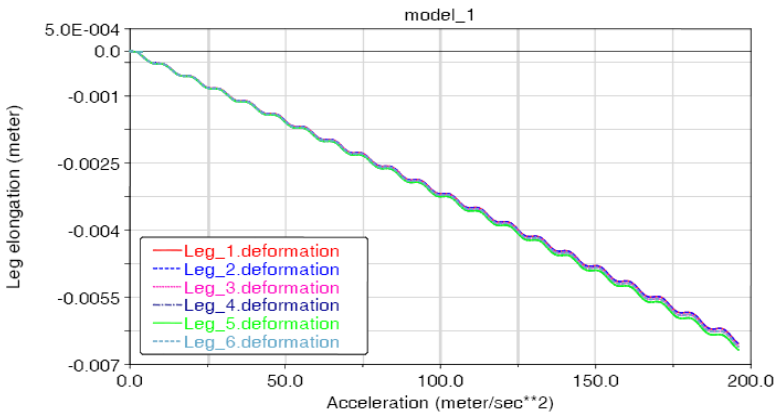

Figure 12: Elongation of Legs due to Input Acceleration in Z.

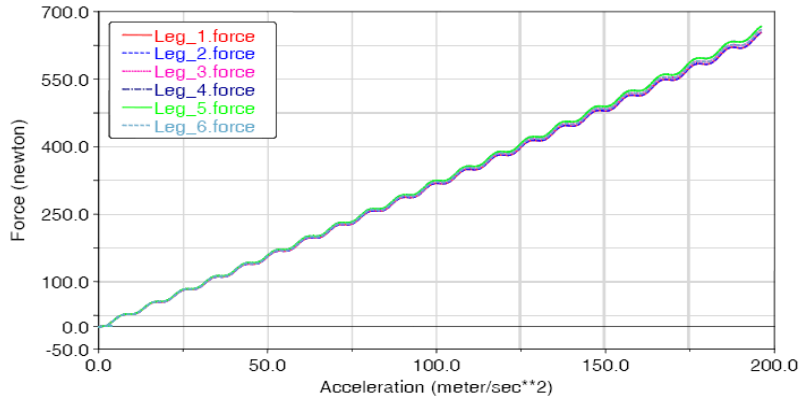

Figure 13: Spring Forces Resisting the QSL Loads in Z axis.

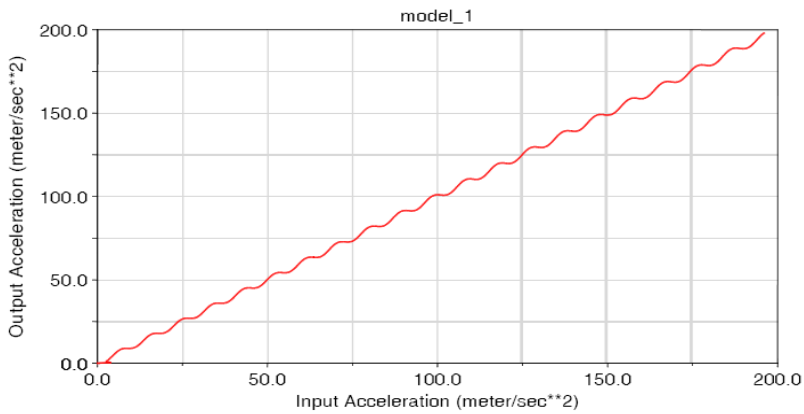

Figure 14: Response of Output Acceleration of Moving Platform.

5.3 Frequency domain analysis for vibration isolation

For vibration isolation of the system a decentralized force feedback PID based control law is implemented. A uniaxial force sensor embedded in the lower part of leg collocated with actuator is used for force feedback. The system performance is assessed by acceleration transmissibility defined between the accelerations of base platform and moving platform. To understand the close loop behavior of the system simulation was carried out using proportional, integral and derivative gains separately and then their combined actions to get suitable performance.

5.3.1 Integral force feedback controls

Integral force feedback using single gains for all loops is implemented. The transfer function of the system defined as ratio of output acceleration at the geometric center of moving platform to input acceleration that is applied at the base as sine sweep of constant magnitude of 50E-3 g up to 1000 Hz. Figure 15 shows the transfer function for Z-axis excitation. The uncontrolled resonance transmissibility can be seen at 22 Hz where there is the plunge mode frequency. No other modes get excited at for this direction input. It can be seen that resonance peak is decreasing as integral feedback gain is increasing and for some gains it is even less then unity upon increasing the gain largely.

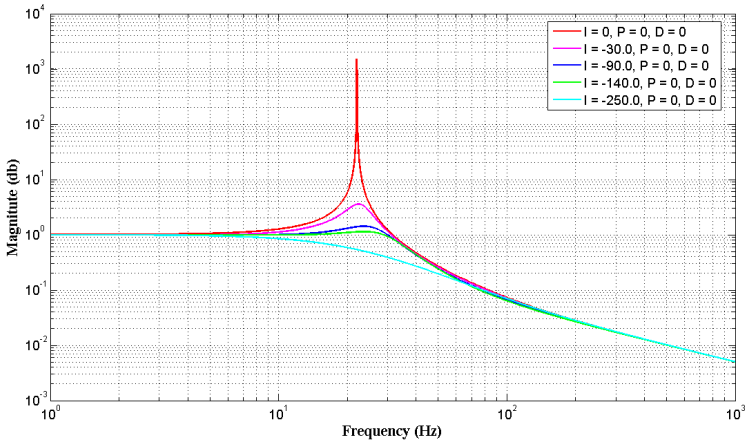

Figure 15: Longitudinal axis Transmissibility for Integral Controller.

A similar transmissibility for X-axis excitation is also obtained and is presented in the Figure 16. Here two modes are excited one at 15 Hz (bending mode) and other around 33 Hz (shear mode). These two excitation frequencies were expected as these are weakly coupled modes. For both axis excitations resonance frequencies of the system remains unaltered but only resonance peaks decreases.

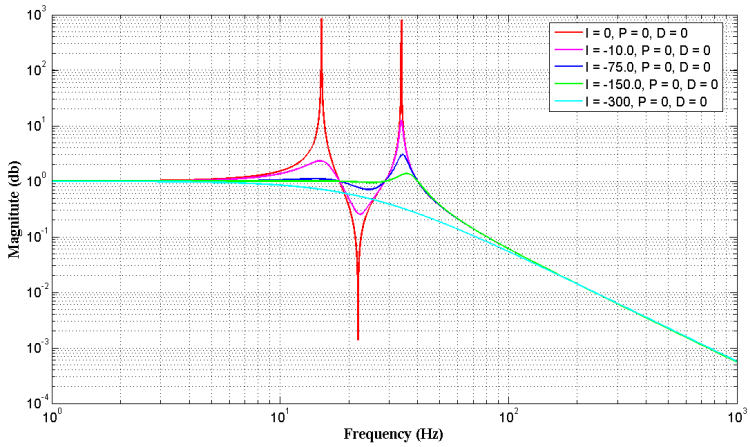

Figure 16: Lateral axis Transmissibility for Integral Controller.

5.3.2 Proportional or derivative force feedback controls

Figures 17-18 presents the transmissibility for X and Z axes with the use of Proportional force feedback controller. It is observed that using Proportional feedback controller has not much effect on resonance transmissibility however shifts the isolation region in higher frequency regime. Figures 19-20 presents the transmissibility for X and Z axes with the use of Derivative force feedback controller. This control strategy has not much effect on resonance transmissibility but significantly shifting the isolation region in lower frequency regime. Since resonance transmissibility is not significantly changing using both the controllers these should always be used with Integral force feedback controller.

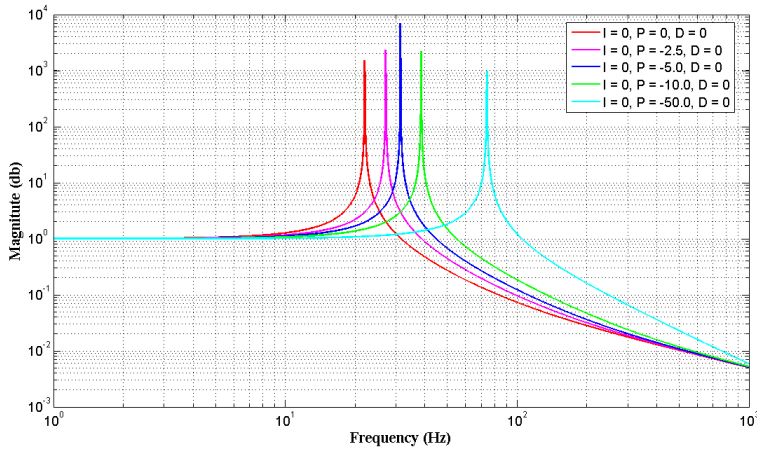

Figure 17: Longitudinal axis Transmissibility for Proportional Controller.

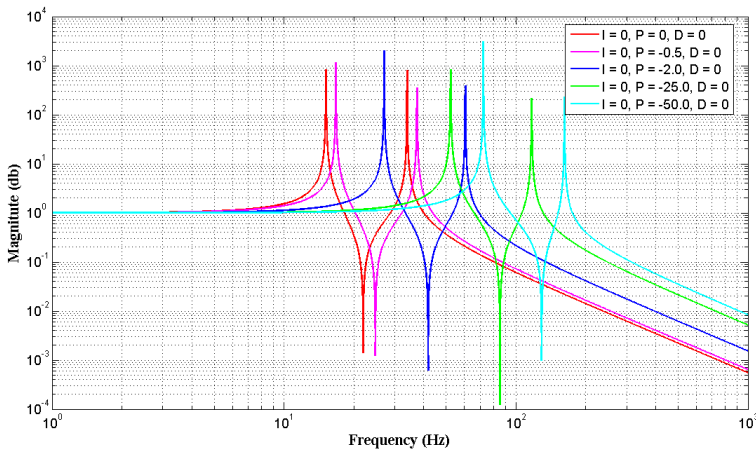

Figure 18: Lateral axis Transmissibility for Proportional Controller.

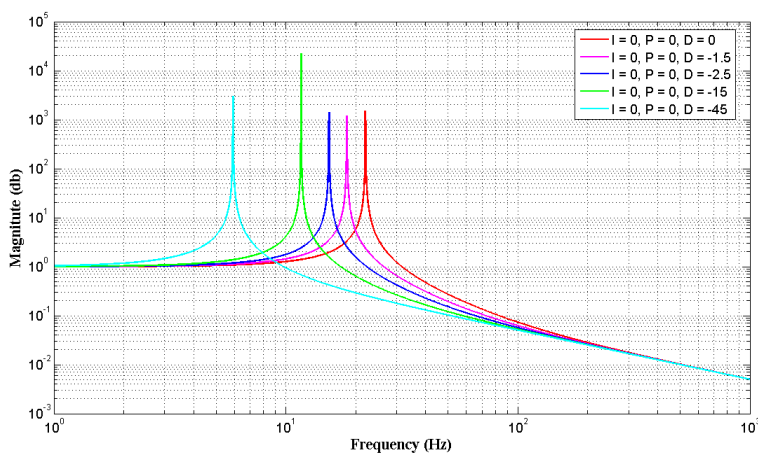

Figure 19: Longitudinal axis Transmissibility for Derivative Controller.

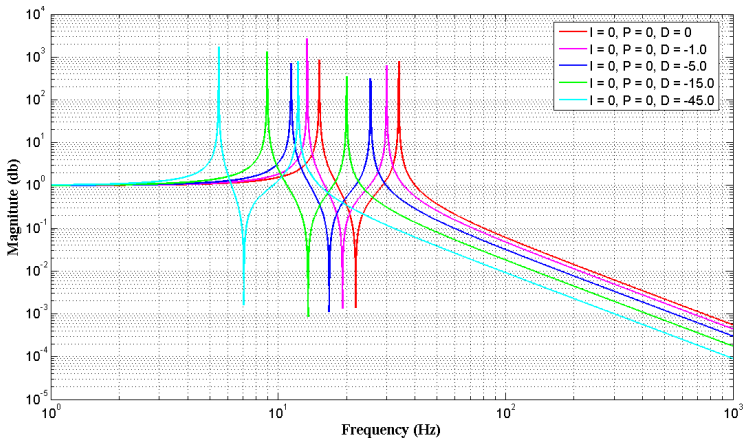

Figure 20: Lateral axis Transmissibility for Derivative Controller.

5.3.3 System performance with PID control

Finally system performance is evaluated with PID control with following gains, $I = -200$, $D = -2$, $P = -2.5$. Figure 21 shows the longitudinal axis transmissibility defined as the relation of the Laplace transforms of the Z axis acceleration at the center of moving platform to the transform of acceleration inputs applied at the center of the base platform. Figure 22 and 24 shows the phase plots with PID controller and without control action for longitudinal and lateral axis transfer functions respectively. Using PID controller a significant reduction in the resonance transmissibility is observed and the natural frequency is also reduced.

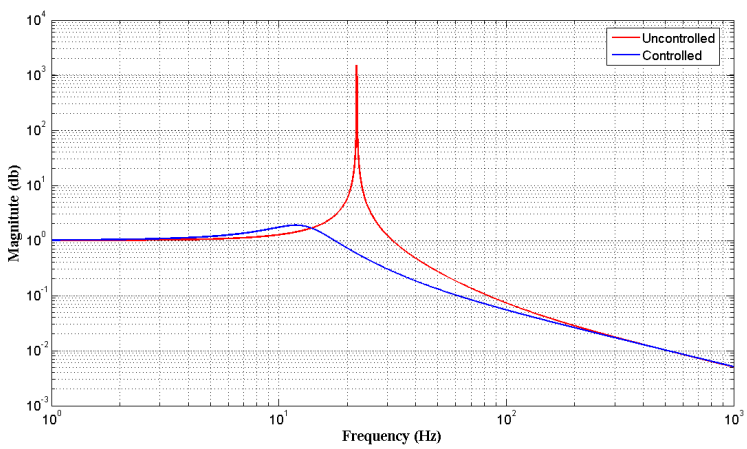

Figure 21: Longitudinal axis Transmissibility using PID controller.

Figure 23 shows the lateral axis transmissibility defined as the relation of the Laplace transforms of the X axis acceleration at the center of moving platform to the transform of acceleration inputs applied at the center of the base platform. The transmissibility defined in this work present a more realistic model as disturbances are acting in all directions. Here again a significant reduction in the transmissibility and natural frequency is observed by using a PID controller at the natural frequencies.

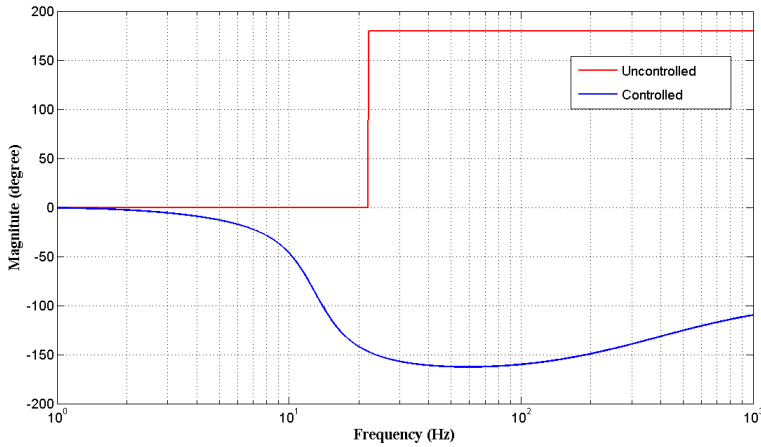

Figure 22: Phase Plot of Longitudinal axis Transfer Function.

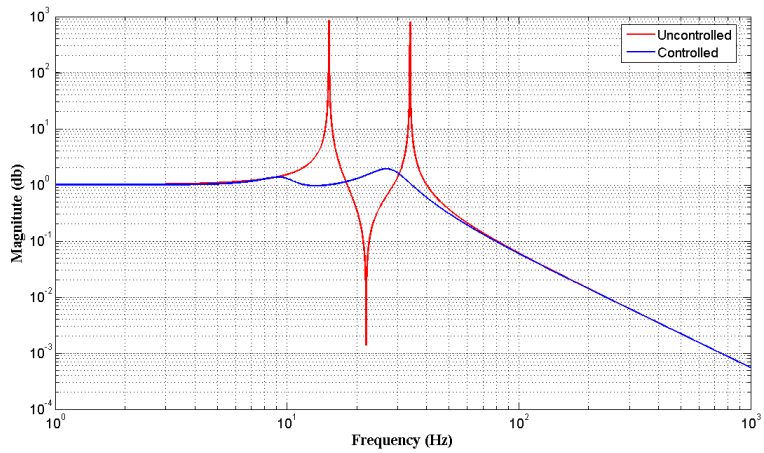

Figure 23: Lateral axis Transmissibility using PID controller.

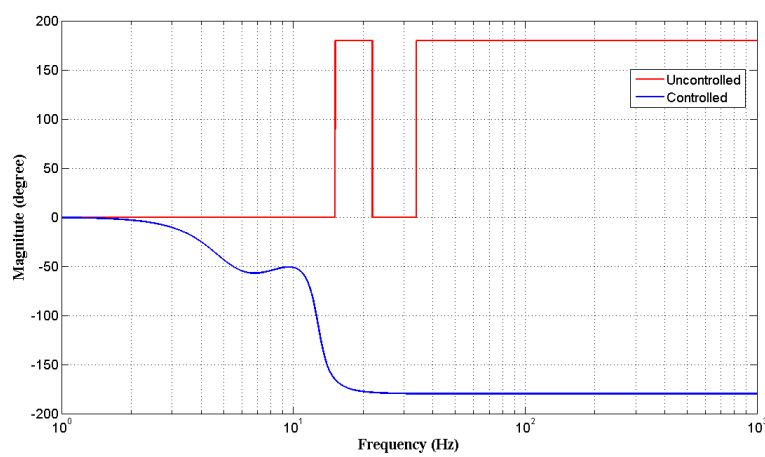

Figure 24: Phase Plot of Lateral axis Transfer Function.

6 CONCLUSIONS

In this paper, modelling and simulation of Stewart platform mechanism, a multi-body system for its vibration control using sensors and actuators is presented. Firstly, kinematic and dynamic modeling based on Newton-Euler formulation is derived for a general class of Stewart platform mechanism. Then, modeling of the mechanism using geometric and inertial properties is done on MSC ADAMS. Finally, the simulation results for the vibration analysis are presented. Simulation results shows different mode shapes when sinusoidal disturbance in the three orthogonal axes is provided. When a proportional feedback controller is applied the resonance transmissibility is not effected even it amplifies on increasing the gain however shifts the isolation region in higher frequency regime. The use of derivative feedback controller reduces the suspension frequency of the mechanism thus increasing the isolation range, however, the resonance transmissibility is not reduced more over a big negative gains even amplifies it. The use of Integral feedback controller reduces the resonance peak monotonically without altering the corner frequencies of the platform. The combined use of PID controller significantly reduces the resonance transmissibility and the natural frequency in the lateral and longitudinal axis when input in 3 orthogonal axes is applied simultaneously.

References

Abu Hanieh, A., Horodinca, M., Preumont, A., (2002). Six-degree-of-freedom hexapods for active damping and active isolation of vibrations. Journal of physics 12(11): 41-48.

Cobb, R.G., Sullivan, J.M., Das, A., Davis, L.P., Hyde, T.T., Davis, T., Rahman, Z.H., Spanos, J.T., (1999). Vibration isolation and suppression system for precision payloads in space. Smart Material and Structures 8: 798–812.

Dasgupta, B., Mruthyunjaya, T.S., (1998). A Newton-Euler formulation for the inverse dynamics of the Stewart Platform manipulator. Mechanism and Machine Theory 33(8): 1135-1152.

Fehr, J., Eberhard, P., (2011). Simulation process of flexible multibody systems with non-modal model order reduction techniques. Multibody Syst Dyn 25: 313–334.

Furqan, M., Alam, M.N., (2013). Finite element analysis of a Stewart Platform using flexible joints. Proceedings of the 1st International and 16th National Conference on Machines and Mechanisms (iNaCoMM2013), IIT Roorkee, India, 1044-1049.

Gallardo, J., Rico, J.M., Frisoli, A., Checcacci, D., Bergamasco, M., (2003). Dynamics of parallel manipulatos by means of screw theory. Mechanism and Machine Theory 38(11): 1113 - 1131.

Geng, Z., Haynes, L.S., Lee, J.D., Carroll, R.L., (1992). On the dynamic model and kinematic analysis of a class of Stewart platforms. Robotics and Autonomous Systems 9(4): 237-254.

Geng, Z., Haynes, L.S., (1993). Six degree-of-freedom active vibration isolation using Stewart platform manipulator. Journal of Robotics Systems 10 (5): 725–744.

Graf, R., Dillmann, R., (1997). Active acceleration compensation using a Stewart platform on a mobile robot. Proc. Euromicro Workshop on Adv. Mobile Robots (EUROBOT): 59–64.

Hajimirzaalian, H., Moosavi, H., Massah, M., (2010). Dynamics analysis and simulation of parallel robot Stewart platform. The 2nd International Conference on Computer and Automation Engineering (ICCAE), Singapore. 5: 472–477.

Hajimirzaalian, H., Ferraresi, C., Moosavi, H., Massah, M., (2013). An analytical method for the inverse dynamic analysis of the Stewart platform with asymmetric-adjustable payload. Proceedings of the Institution of Mechanical Engineers, Part K: Journal of Multi-body Dynamics 227(2): 162-171.

Harib, K., Srinivasan, K., (2003). Kinematic and dynamic analysis of Stewart platform-based machine tool structures. Robotica 21: 541-554.

Hayat, A.A., Akhlaq, A., Alam, M.N., (2012). Design of a flexural joint using finite element methods. Machines and Mechanism: 198-205.

Hongling, S., Kun, Z., Haibo, C., Peiqiang, Z., (2007). Improved Active Vibration Isolation Systems. Tsinghua Science and Technology ISSN 1007-0214 05/19 12(5): 533-539.

Hoque, M.E., Mizuno, T., Ishino, Y., Takasaki, M., (2010). A six-axis hybrid vibration isolation system using active zero-power control supported by passive weight support mechanism. Journal of Sound and Vibration 329: 3417–3430.

Hoque, M.E., Mizuno, T., Ishino, Y., Takasaki, M., (2011). A three-axis vibration isolation system using modified zero-power controller with parallel mechanism technique. Mechatronics 21: 1055-1062.

Kapur, P., Ranganath, R., Nataraju, B.S., (2007). Analysis of Stewart platform with flexural joints at singular configurations. 12th IFToMM World Congress, Besançon (France).

Lebret, G., Liu, K., Lewis, F.L., (1993). Dynamic analysis and control of a Stewart Platform manipulator. Journal of Robotic Systems 10(5): 629-655.

Li, B., Zhao, W., Deng, Z., (2012). Modeling and analysis of a multi-dimensional vibration isolator based on the parallel mechanism. Journal of Manufacturing Systems 31: 50-58.

Liu, M.J., Li, C.X., Li, C.N., (2000). Dynamics analysis of the Gough-Stewart Platform manipulator. IEEE Transactions on Robotics and Automation 16(1): 94-98.

Liu, L., Benli, W., (2008). Multi objective robust active vibration control for flexure jointed struts of Stewart Platforms via H∞ and μ synthesis. Chinese Journal of Aeronautics 21: 125-133.

Lopes A.M., (2009). Dynamic modeling of a Stewart platform using the generalized momentum approach. Communications in Nonlinear Science and Numerical Simulation 14(8): 3389 - 3401.

MSC.Software Corporation:Msc Adams Version 2010.

Mukherjee, P., Dasgupta, B., Mallik, A.K., (2007). Dynamic stability index and vibration analysis of a flexible Stewart platform. Journal of Sound and Vibration 307: 495-512.

Preumont, A., Horodinca, M., Romanescu, I., de Marneffe, B., Avraam, M., Deraemaeker, A., Bossens, F., Abu Hanieh, A., (2007). A six-axis single-stage active vibration isolator based on Stewart platform. Journal of Sound and Vibration 300: 644-661.

Stewart, D., (1965) A platform with six degree of freedom. Proceedings of the Institution of Mechanical Engineers 180 Part 1: 371 - 386.

Wang, W., Yang, H., Zou, J., Ruan, X., Fu, X., (2009). Optimal design of Stewart platforms based on expanding the control bandwidth while considering the hydraulic system design. Journal of Zhejiang University SCIENCE A 10(1): 22-30.

Xia, Y., Pang, J., Hu, C., Zhou, C., Wu, C., (2014). Multi-body dynamic analysis of driveline torsional vibration for an RWD vehicle. SAE Technical Paper 2014-01-2064, 8th International Styrian Noise, Vibration & Harshness Congress: The European Automotive Noise Conference.

Zhang, Q., Fan, X., Zhang, X., (2014). Dynamic analysis of planar 3-RRR flexible parallel robots with dynamic stiffening,. Shock and Vibration 2014, Article ID 370145, 13 pages.